Penerbit Akademia Baru

Journal of Advanced Research in Fluid Mechanics and Thermal Sciences

Journal homepage: www.akademiabaru.com/arfmts.html
ISSN: 2289-7879

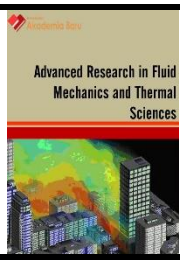

Interaction Effect of Process Variables on Solar-Assisted Photocatalytic Phenol Degradation in Oilfield Produced Water Over ZnO/Fe_2O_3 Nanocomposites

Open Access

Omer Al Haiqi [1,*], Abdurahman Hamid Nour[1], Bamidele Victor Ayodele[2], Rushdi Bargaa[1]

[1] Faculty of Chemical and Process Engineering, Technology, Universiti Malaysia Pahang, Malaysia
[2] Institute of Energy Policy and Research, Universiti Tenaga Nasional, Jalan IKRAM-UNITEN 43000, Kajang Selangor, Malaysia

ARTICLE INFO

Article history:
Received 19 April 2020
Received in revised form 20 September 2020
Accepted 22 September 2020
Available online 26 November 2020

ABSTRACT

This study investigates the interaction effects of process variables on photocatalytic phenol degradation in oil produce water. A series of ZnO/Fe_2O_3 nanocomposite prepared using the sol-gel method and calcined at a temperature range of 400-600 °C were employed as photocatalysts. The characterization analysis using different instrument techniques revealed that the ZnO/Fe_2O_3 nanocomposites have suitable physicochemical properties as photocatalysts. The photocatalytic activity of the ZnO/Fe_2O_3 nanocomposite was examined in photo-reactor considering the degradation of the phenol and the reduction in chemical oxygen demand (COD) in the oilfield produced water under direct sunlight. It was ascertained that process variables such as irradiation time, calcination temperature of the ZnO/Fe_2O_3 nanocomposites, and the ZnO/Fe_2O_3 nanocomposites concentration significantly influenced the chemical oxygen demand and phenol removal. Based on the analysis of variance (ANOVA), the effects of the process variables on the phenol and COD removal can be ranked as irradiation time (p-value < 0.0001) > calcination temperature of the ZnO/Fe_2O_3 nanocomposite (p-value = 0.0003) > ZnO/Fe_2O_3 concentration (p-value = 0.0013). The interaction between the parameters was observed to have a substantial effect on COD and phenol removal. However, the interaction effect that produced the most significant influence on the COD and phenol removal was recorded between the irradiation time and the ZnO/Fe_2O_3 nanocomposite concentration.

Keywords:
Box Behnken Design; Interaction effects; Oil field produced water; ZnO/Fe_2O_3 nanocomposite; photocatalytic degradation

1. Introduction

Produced water from the oil field consists of a mixture of dissolved and particulate organic and inorganic toxic substances such as aromatic hydrocarbons, alkylphenols, some traces of heavy

* *Corresponding author.*
E-mail address: omaralhaigi@gmail.com

https://doi.org/10.37934/arfmts.78.1.100121

metals, and so on [1]. If this oil field produced water is not properly treated before their discharge into water bodies, it might pose a serious health risk to both marine lives and human [2,3]. Marine lives often bioaccumulate these toxic substances (heavy metals, phenols, and hydrocarbons) as a result of their contacts with the water bodies containing the discharged untreated oilfield produced water [4]. Amongst these toxic pollutants, phenol has been reported to be one of the most hazardous in terms of health risk [5,6]. Reports have shown that the total concentration of phenol in oil field produced water is often less than 20 mg/L which is far more than the World Health Organization recommended concentration of 0.02 µg/L for treated water [7]. Due to the environmental impacts and the health effects of untreated oil field produced water discharged into water bodies, regulatory agencies in different countries with oil and gas platform have placed limits on the minimum allowable concentrations of these toxic substances in oil field produced water before being discharged into water bodies [1]. These limits or standard differs from country to country.

To attain the minimum limits of these recalcitrant organic and inorganic toxic substances, the oil field produced water is often treated using several methods. An extensive review by Ahmadun *et al.,* [1] revealed that oil field produced water can be treated by physical, chemical, and biological methods as well as, the combinations of any two or all the methods. The physical treatment entails the adsorption of the dissolved organic compounds unto porous materials such as activated carbon, organoclay, resin, co-polymers, and zeolites [2,8–12]. Although, the physical treatment of oil field produced water has been adjudged to be effective to a large extent, nevertheless, has not been that effective to remove recalcitrant organic compounds such as phenol. The biological treatment has also been employed for the treatment of the oil field produced water before discharge into water bodies [13–15]. The biological treatment techniques entail the use of aerobic or anaerobic microorganism for the degradation of organic and inorganic compounds in the oil field produced water [15]. Due to the sensitivity of the microorganism, biological treatment is usually very complex to control. Chemical treatment methods such as precipitation using a coagulant, chemical oxidation, electrochemical process, photocatalytic treatment, Fenton process, treatment with ozone, room temperature ionic liquids, and demulsifier [16–22]. Amongst all these chemical treatment methods, the treatment of oil field produced water using photocatalytic techniques is receiving growing attention due to its numerous advantages which include simple handling of the process and the inexpensive nature of the photocatalysts [23,24]. The photocatalytic degradation of an organic and inorganic toxic substance is a form of redox reaction which occurs via light radiation resulting in the generation of electrons and holes. In the course of the photocatalytic reaction, the toxic compounds are degraded to carbon dioxides and water by hydroxyl radicals and superoxides produced by the electrons and holes [24].

An extensive review by Ani *et al.,* [25] revealed that several photocatalysts such as ZnO, ZnS, Fe_2O_3, CdS, SiO_2, and TiO_2 have been employed for the degradation of organic compounds in the oil produced water. These photocatalysts have been reported to show great potentials in degrading organic substances in an oil field produced water. Besides, photocatalysts such as CeO_2 and gold nanoparticles have been reported as good photocatalytic candidates for degradation of organic pollutants [26–28]. The excellent performance of ZnO and Fe_2O_3 as photocatalyst for degradation of organic pollutants in an oil field produced water has been reported by Vaiano *et al.,* [29] and Xie *et al.,* [30]. Their performance was attributed to their long-term stability and exceptional charge transport properties. However, photocatalytic activity occurs mostly at ultra-violet (UV) light regions with bandgap less than 3 eV. Further modifications of the ZnO and Fe_2O_3 into a composite structure could enhance the absorption of light within the visible light region. This would enable the vast solar resources mostly in the visible region be harnessed for the photocatalytic treatment of the oil field produced water. The present study therefore explored the synergistic effects of using ZnO/Fe_2O_3

nanocomposite for degradation of organic pollutant in oil field produced water under direct sunlight. The effects of process parameters such as irradiation time, calcination temperature of the ZnO/Fe_2O_3 nanocomposite, the ZnO/Fe_2O_3 concentration on photodegradation of the toxic organic substance in oil field produced water were investigated using Box-Behnken Design of Experiment (BBDoE). Box Behnken design of experiment is a robust technique used for investigating the interaction effects of process parameters on the output variables. The use of BBDoE to investigate the effect of irradiation time, methane concentration, steam concentration on photocatalytic hydrogen production by steam reforming has been reported by Ayodele *et al.,*.

2. Methodology

2.1 Oil Field Produced Water Collection

The oil field produced water used in this study was collected from a treatment plant in Masila, Yemen. The water sampled was collected in an airtight dark bottle and kept in a refrigerator before its physicochemical analysis. The oil field produced water was subsequently characterized to determine the concentration of phenol. Table 1 shows the concentration of the phenol and other physicochemical properties of the oil field produced water.

Table 1
Physicochemical properties of the oil field produced water

Conductivity, uS/cm	37,200
TDS, mg/l	24,552
Suspended solids (mg/l)	731
pH	6.80
Nitrate (NO_3). mg/l as N	0.01
Phenol, mg/L	4.50
Oil in Water Content, ppm	18.00
COD, mg/L	650

2.2 Materials

The starting materials for the preparation of the of ZnO/Fe_2O_3 nanocomposite photocatalyst are Zinc nitrate hexa-hydrate ($Zn(NO_3)_2.6H_2O$, 99.999% trace metal bases, Sigma-Aldrich), iron **(**III) nitrate nonahydrate ($Fe(NO_3)_3.9H_2O$, 99.999% trace metal bases, Sigma-Aldrich), ethanol (90% by volume), ethylene glycol, hydrochloric acid, and citric acid. All the chemicals were analytic grade and used without any modification.

2.3 Preparation of Photocatalysts

The ZnO/Fe_2O_3 nanocomposite photocatalyst was synthesized using the sol-gel method in accordance with the method of Li *et al.,* [31]. Sol-gel method of photocatalyst synthesis is a wet-chemical route which significantly influences the nanostructure of any catalytic materials [32]. Firstly, a molar ratio of 1:3 $Zn(NO_3)_2.6H_2O$ and $Fe(NO_3)_3.9H_2O$ precursors were dissolved in a beaker containing 100 ml ethanol and mixed thoroughly for 30 min. A separate mixture of 3 mol of citric acid and 50 ml ethanol was prepared and subsequently added to the solution containing the precursors to form a colloidal gel-like solution. The overall mixture was continuously stirred at a constant temperature of 60 ^oC on a hot plate for 60 min to complete the hydrolysis and condensation with intermittent addition of NH_3 and HCl to adjust the pH of the gel. The gel was dried in the oven at 80 ^oC for 40 min to obtain a porous material referred to as xerogel. The xerogel was subsequently

calcined for 3 h at temperature range of 400-600 °C to obtain the as-prepared ZnO/Fe_2O_3 nanocomposite photocatalyst.

2.4 Characterization of ZnO/Fe_2O_3 Photocatalysts

The as-prepared ZnO/Fe_2O_3 photocatalysts were examined for their physicochemical properties using an X-ray Diffractometer (XRD), Transmission Electron Microscope (TEM), Field Emission Scanning Electron Microscope (FESEM), N_2 physisorption analysis and UV/Vis spectrophotometer, thermogravimetric analysis (TGA). The detailed procedures of each of the characterization techniques are described below.

The phase identification and crystallinity of the ZnO/Fe_2O_3 nanocomposite were determined using the Panalytic Alx Pert Powder X-ray Diffractometer coupled with X'Celerator. A Cu Kα radiation of 1.5406 Å was employed. A rotary plate was used for the preparation of the powder samples. The XRD pattern of the ZnO/Fe_2O_3 nanocomposite was determined by scanning the samples in 2θ range of 20 to 80° at a rate of 0.2 °/sec. The crystallite size, D was calculated based on the Scherrer formula shown in Eq. (1). EVA software (version 2) was used to identify the structure and lattice strain of the samples. The XRD patterns of all samples were compared with the Joint Committee on Powder Diffraction Standards (JCPDS), which is a standard from the software library.

$$D = \frac{K\lambda}{\beta \cos\theta} \tag{1}$$

where K is the Scherer constant (K=0.89), λ is the X-ray wavelength, β is the peak width of half maximum, and θ is the Bragg diffraction angle.

The microstructure of the as-synthesized ZnO/Fe_2O_3 nanocomposite was determined by TEM on a TECNAL G2F20 TEM machine with a working voltage of 200 kV. Before the analysis, about 5 mg of the ZnO/Fe_2O_3 samples were dispersed in ethanol and thereafter sonicated for 20 min. The sonicated sample was deposited on a Copper grid with the aid of a holy carbon film. The morphology of ZnO/Fe_2O_3 nanocomposite was investigated by Field Emission Scanning Electron Microscope (FESEM Model: JEOL, JSM-7800F Japan). The elemental distribution of the nanocomposite was investigated by energy-dispersive X-ray (EDX), an integral component of the JEOL, JSM-7800. All samples were coated with platinum using the Sputter Coater model JFC-1600 to prevent or reduce electrical charging during testing.

The specific surface area and the pore distribution of the ZnO/Fe_2O_3 nanocomposite were measured by N_2 physisorption analysis using Micromeritics ASAP 2020 Accelerated Surface Area and Porosimetry System. Before the analysis, 0.1 to 0.3 g of sample was degassed under nitrogen at 350°C for some hours to remove any water or humidity from the sample. The specific surface area and pore distribution of the nanocomposite were obtained in the range of 0.05-0.3 for (P/P^o) relative pressure from the adsorption-desorption isotherm using Brunauer-Emmett-Teller (BET) and BJH methods. The total adsorption of nitrogen was used to determine the volume and the average size of the pore.

The bandgap of the ZnO/Fe_2O_3 nanocomposite was measured by diffuse reflectance spectrophotometric analysis on a UV/Vis spectrophotometer (Shimadzu Model: UV-2600, Japan). The spectra were recorded at room temperature with the wavelength ranging from 200–800 nm. The scans of spectrophotometer were collected in a slow-speed mode for all samples. The halogen lamp and deuterium lamp at 390 nm was supplied as a light source. The baseline correction was performed using a calibrated sample of barium sulphate ($BaSO_4$) as a standard. The liquid sample also runs to

determine the wavelength absorbance of pollutants and efficiency in removing colour pollutants. The samples were run with slow speed at 0.2 nm intervals and 0.5 nm as slit width. One set of quartz cells with 5 ml volume was used to perform all experiment runs. The deionized water was used as a blank solution with all the samples.

The thermal stability of ZnO/Fe_2O_3 nanocomposite as a function of temperature was determined by TGA using Thermal analyzer (STA 7000, Hitachi, Japan). The TGA analysis of the ZnO/Fe_2O_3 nanocomposite was performed by measuring about 15 mg of the sample into alumina pan. The sample was heated gradually, from room temperature at a heating rate of 10°C/min to 800°C. The percentage weight loss of the ZnO/Fe_2O_3 nanocomposite as a function of temperature was obtained from the data generated from the TGA analysis.

2.5 Photocatalytic Degradation Activity

The photocatalytic degradation activity of the ZnO/Fe_2O_3 nanocomposite was investigated to determine the extent of degradation of the toxic pollutants which majorly consists of phenol. The interaction effects of parameters such as irradiation time, ZnO/Fe_2O_3 concentration, and calcination temperature on percentage phenol degradation and percentage COD removal were investigated using BBDoE. The BBDoE details are shown in Table 2. The photocatalytic degradation experimental runs were performed in a cylinder batch reactor (non-concentrating type slurry reactor). 120 ml of the reactor was used to perform all the experiments, during which each volume of 100 ml was used. A specified amount of ZnO/Fe_2O_3 nanocomposite equivalent to 0.5-5 mg/L was added to the oil field produced water and continuously stirred under dark for 60 minutes. Thereafter, the mixture was exposed to direct sunlight to initiate the photoreaction. 0.5 to 1.0 ml of the aliquots obtained after a particular degradation time was collected at a 15 min interval, centrifuged, and then filtered. High-performance Liquid Chromatography (486- WFMA HPLC) was employed to determine the concentration of the non-degraded toxic compound. The HPLC consists of Genesis C18 Colum with a dimension of 250 mm x 4.6 mm x 4 µm and a variable wavelength UV detector was employed to measure the concentration of phenols before and after the photocatalytic degradation. Acetonitrile: water solution (20:80 v/v) and 0.01 M phosphoric acid (H_3PO_4) as the mobile phase with a flow rate of 1.0 ml/min were applied. The photocatalytic degradation efficiency (DE %) of toxic compounds was calculated using Eq. (2).

$$DE\% = \frac{C_0 - C}{C_0} \times 100 \tag{2}$$

where C_o is the initial concentration at t = 0 and C is the concentration of toxic compounds at different intervals of irradiation time, $t = t_{min}$.

Furthermore, 2 ml of the samples after 15 min irradiation were withdrawn for Chemical Oxygen Demand (COD) analysis. The COD tests were carried out according to close reflux, colorimetric method, using HACH DR/2010 Spectrophotometer with a COD reactor. A 2 ml of solution sample before and after treatment was added to high range (HR: 150-1500 mg/l) of reagent consists of potassium dichromate solution ($K_2Cr_2O_7$). Before the COD analysis, the final solution was heated at 150°C in a digestion reactor for 2 h and thereafter allowed to cool to room temperature. The COD of the aliquot was subsequently measured by spectroscopic, according to the concentration of Cr^{3+} produced from the reaction at an absorbance wavelength of 420 and 620 nm for LR and HR respectively. COD removal was calculated using Eq. (3).

$$CODR\% = \frac{\mathrm{COD_o} - \mathrm{COD}}{\mathrm{COD_o}} \times 100 \quad (3)$$

where COD_o is before degradation at t = 0 and COD is after degradation of phenol at different intervals of irradiation time, t = t_{min}.

Table 2
Detailed parameters used for the BBDoE

Variables	Unit	Low level	High level
ZnO/Fe_2O_3 concentration	mg/L	1	3
Irradiating time	min	20	160
Calcination temperature	°C	400	600

3. Results and Discussions

The analysis of the produced water in oilfield shows that the initial phenol and COD before the photocatalytic treatment was 4.5 mg/L and 650 mg/L, respectively as shown in Table 1.

3.1 Characterization of The ZnO/Fe_2O_3 Nanocomposite

The XRD pattern of the ZnO/Fe_2O_3 nanocomposite calcined at 400 °C, 500 °C, and 600 °C are depicted in Figure 1. The reflection peaks from the XRD pattern are well indexed to the cubic structure of $Fe_{2.02}O_4Zn_{0.96}$ nanocomposite with corresponding lattice constants of a = b = c = 8.456 (ICDD no: 98-008-9727). Both ZnO and Fe_2O_3 were not identified as they aggregated to form $Fe_{2.02}O_4Zn_{0.96}$ nanocomposite [30]. However, the reflection peaks of the ZnO/Fe_2O_3 nanocomposite obtained from the XRD pattern are strongly influenced by the calcination temperature. The diffraction peaks of ZnO/Fe_2O_3 nanocomposite calcined at 400 °C is seen to be broader compared to those calcined at 500 °C and 600 °C.

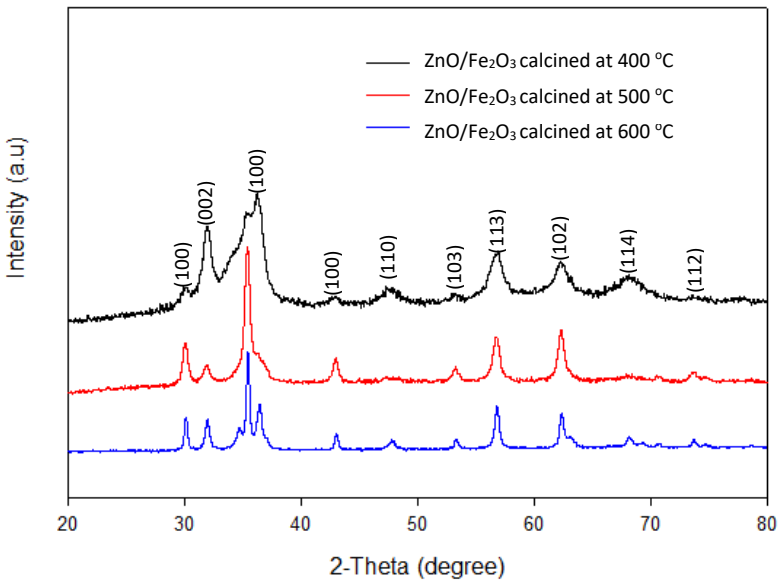

Fig. 1. XRD pattern of the ZnO/Fe_2O_3 nanocomposite calcined at different temperature

The adsorption-desorption isotherm of the ZnO/Fe_2O_3 nanocomposites obtained from the N_2 physisorption analysis is depicted in Figure 2. The analyzed ZnO/Fe_2O_3 nanocomposites calcined at temperature ranged of 400-600 °C showed a typical characteristic of Type IV adsorption isotherm with H3-hysteresis loop based on IUPAC classifications of mesoporous materials [33,34]. The type IV adsorption isotherm indicates that the liquid N_2 was weakly adsorbed onto the surface of the ZnO/Fe_2O_3 nanocomposites with an occurrence of capillary condensation in the mesopores of the samples [35].

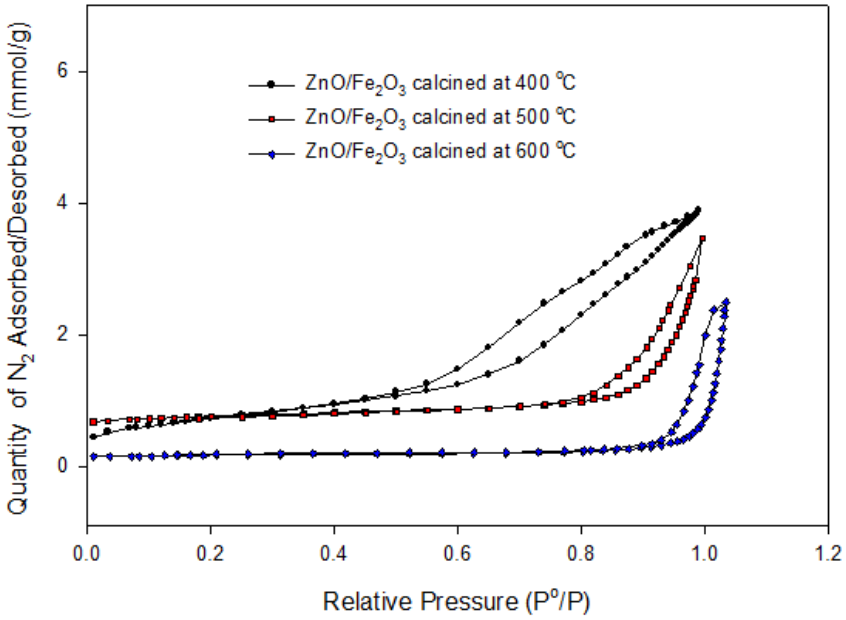

Fig. 2. Adsorption-Desorption isotherm of the ZnO/Fe_2O_3 nanocomposite calcined at a temperature range of 400 °C-600 °C

The BET specific surface area and the BJH pore distributions of the ZnO/Fe_2O_3 nanocomposites are presented in Table 3. It can be seen that the specific surface area of the ZnO/Fe_2O_3 nanocomposites decreases with an increase in the calcination temperature. The ZnO/Fe_2O_3 nanocomposites calcined at 400 °C gave the highest BET specific surface area of 57.64 m^2/g while that calcined at 600 °C gave the lowest BET surface area of 7. 67 m^2/g. The decrease in the BET specific surface area of the ZnO/Fe_2O_3 nanocomposites is an indication of the effect of calcination temperature of the textural properties of catalytic materials. Similarly, the cumulative pore volume of the ZnO/Fe_2O_3 nanocomposites also decreases with increase in the calcination temperature. The highest and lowest pore volume of 0.137 cm^3/g and 0.078 cm^3/g were obtained for the ZnO/Fe_2O_3 nanocomposites calcined at 400 °C and 600 °C, respectively. The mesoporous nature of the ZnO/Fe_2O_3 nanocomposites is evidence from the values of the average pore diameter which were estimated as 9.34, 24.60, and 50.92 for ZnO/Fe_2O_3 nanocomposites calcined at 400 °C, 500 °C and 600 °C respectively. For a mesoporous material the average pore diameter must the greater than 2 nm.

Table 3
Textural properties of the ZnO/Fe_2O_3 nanocomposite calcined at different temperature

Photocatalysts	BET specific surface area (m^2/g)	Cumulative pore volume (cm^3/g)	Average pore diameter (nm)
ZnO/Fe_2O_3 calcined at 400 °C	57.64	0.137	9.34
ZnO/Fe_2O_3 calcined at 500 °C	20.72	0.126	24.60
ZnO/Fe_2O_3 calcined at 500 °C	7.67	0.078	50.92

The morphological and the elemental composition of the ZnO/Fe_2O_3 nanocomposite obtained from the FESEM images and the EDX micrograph are depicted in Figure 3. The ZnO/Fe_2O_3 calcined at 400 °C resulted in a cluster of spherical nanocomposites with average particle sizes of 29.12 nm. As the calcination temperature of the ZnO/Fe_2O_3 nanocomposites increases from 500 °C to 600°C, an agglomeration of spherical nanocomposites with average particle diameters of 56.1 nm, and 57.02 nm respectively were observed. It is obvious that the increase in the calcination temperature of the ZnO/Fe_2O_3 nanocomposites increased the particle size. The elemental make-up of the ZnO/Fe_2O_3 nanocomposites which consist of Zn, O, and Fe are well captured by the EDX micrograph. This further ascertains the robustness of the sol-gel techniques used for the preparation of the ZnO/Fe_2O_3 nanocomposites [36,37]. To further establish the microstructure of the ZnO/Fe_2O_3 nanocomposites, the TEM images of the samples were captured as shown in Figure 4. The TEM images of the ZnO/Fe_2O_3 nanocomposites calcined at temperature ranges of 400-600 °C are depicted in Figure 3. The average sizes of the ZnO/Fe_2O_3 nanocomposite calcined at 400 °C, 500°C, and 600 °C were measured to be 31.4, 51.5 nm, and 57.02 nm, respectively. It is obvious that the nanocomposite sizes increase with an increase in calcination temperature.

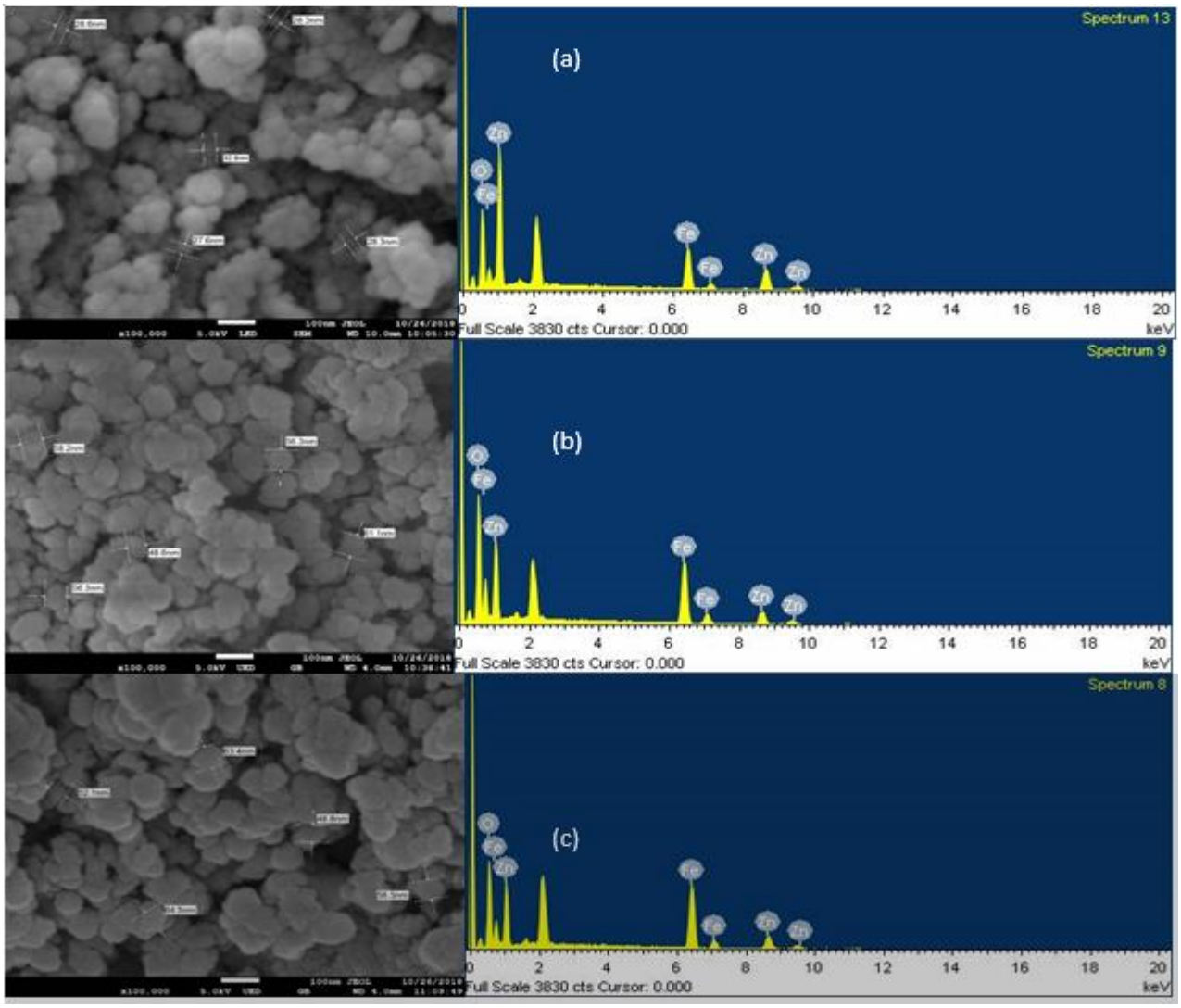

Fig. 3. The FESEM images and EDX micrographs of the ZnO/Fe_2O_3 nanocomposite calcines at (a) 400 °C (b) 500 °C and (c) 600 °C

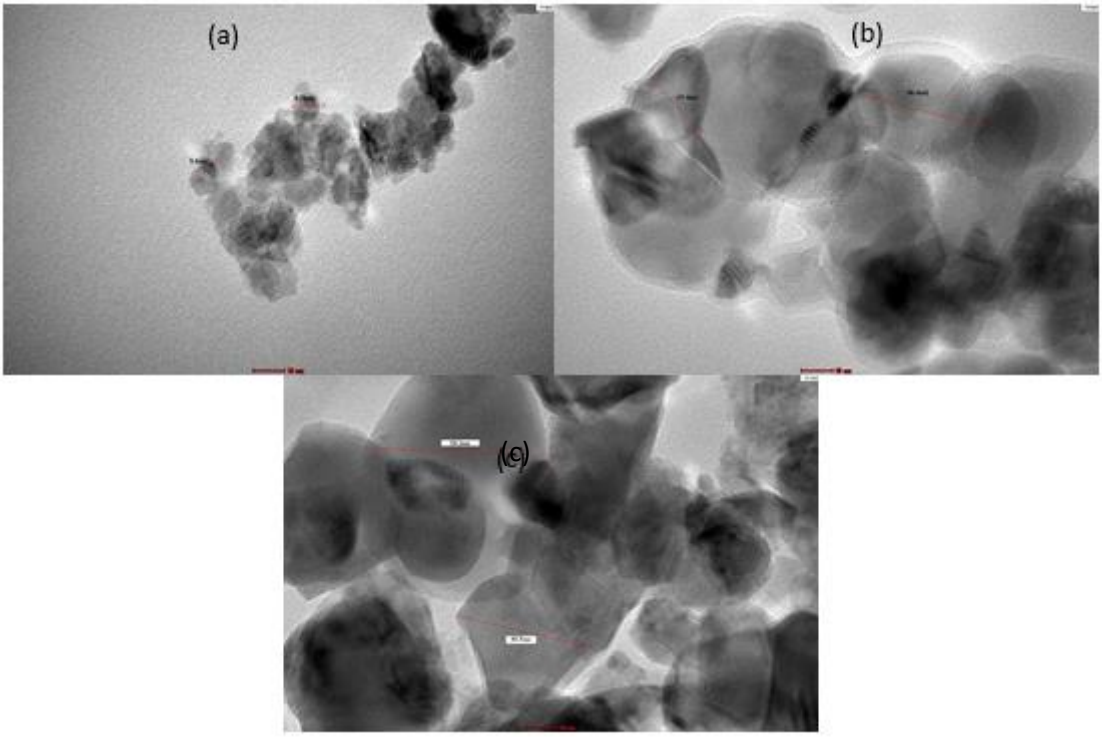

Fig. 4. TEM images of the ZnO/Fe_2O_3 nanocomposites calcined at (a) 400 °C (b) 500 °C (c) 600 °C

The UV-vis absorption spectra of the ZnO/Fe_2O_3 nanocomposites calcined at a temperature range of 400 °C-600 °C are depicted in Figure 5. The three samples of the ZnO/Fe_2O_3 nanocomposites displayed a strong absorption peak in both the ultra-violet region (300-400 nm) and the visible region (400-780) which makes the ZnO/Fe_2O_3 nanocomposites suitable as materials for photocatalytic degradation of organic pollutants in produced water harnessing the vast potential solar energy resources in the visible light region. The band gap of the ZnO/Fe_2O_3 nanocomposites calcined at 400 °C. 500 °C, and 600 °C were estimated as 2.76 eV 2.88 eV and 2.95 eV, respectively.

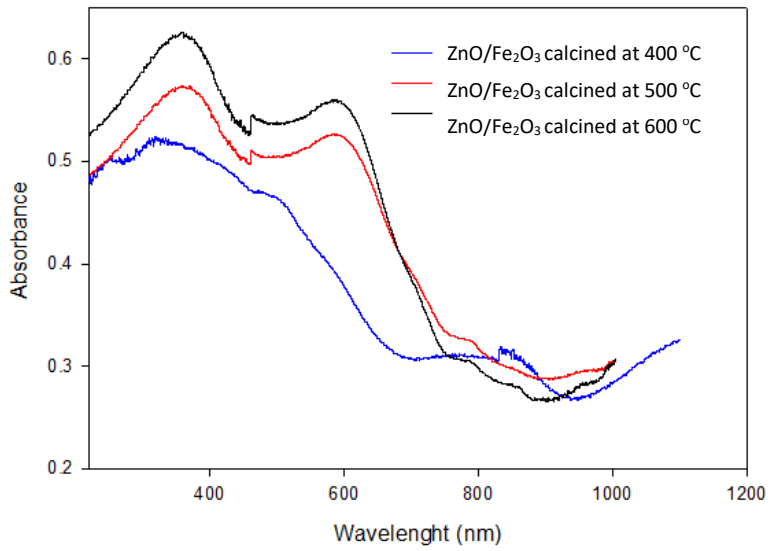

Fig. 5. UV-vis absorption spectra of the ZnO/Fe_2O_3 nanocomposites calcined at temperature ranges of 400 °C – 600 °C

The thermogravimetric (TG) and differential thermogravimetric (DTG) profiles of the ZnO/Fe_2O_3 nanocomposites calcined at temperature ranges of 400 °C – 600 °C is depicted in Figure 6. The evaporation of moisture can be attributed to the small peaks between 100-160 °C in all the three samples. The peaks at the temperature range of 200-300 °C can be attributed to the sequential removal of water of crystallization present in the ZnO and Fe_2O_3 precursors resulting in the formation of the anhydrous nitrate compound of the precursors. Complete decomposition of the anhydrous nitrate compound can be observed at peak range 320-350 °C for all the samples. At the temperature greater than 400 °C, the TG and DTG profiles were completely flattened, an indication of the formation of pure ZnO/Fe_2O_3 nanocomposites which can be substantiated by the XRD and EDX analysis in Figure 1 and 3 respectively.

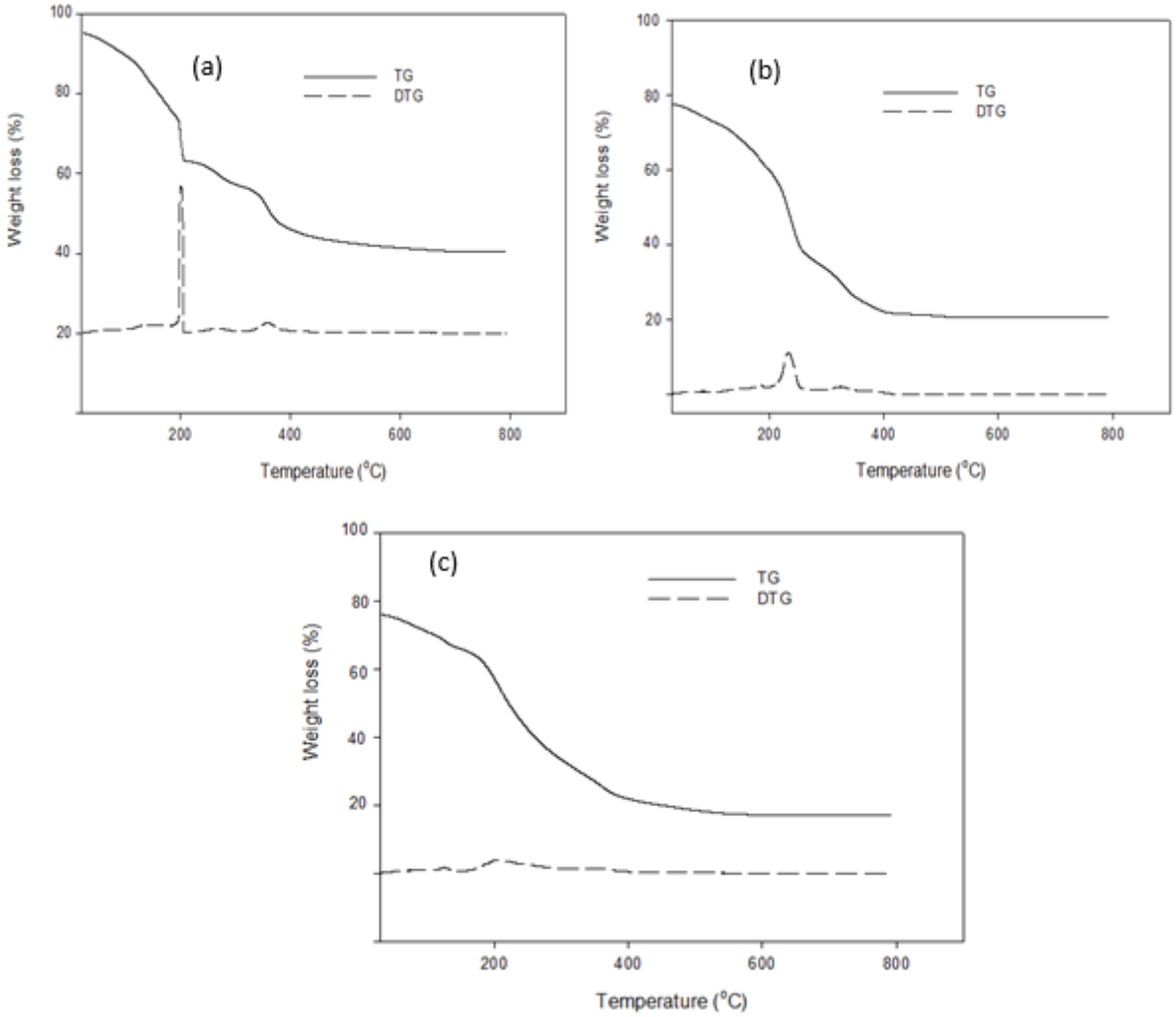

Fig. 6. TG and DTG profiles for the ZnO/Fe_2O_3 nanocomposites calcined at (a) 400 °C (b) 500 °C (c) 600 °C

3.2 Interaction Effects of The Process Parameters on The Percentage COD Removal

The effects of three different parameters namely, irradiation time (min), ZnO/Fe_2O_3 concentration (mg/L), and Calcination temperature (°C) on the percentage COD removal were investigated using Box Behnken Design of Experiment (BBDoE). The interaction effects of a set of two parameters on response was investigated by fixing the third parameter. The three-dimensional plots

showing the effects of these parameters on the COD removal are depicted in Figure 7- 9. The significant effects of the parameters on the COD removal were measured using statistical parameters such as p-value, F-value, lack of fit, coefficient of determination obtained from the analysis of variance (ANOVA) [38]. At a fixed calcination temperature of 400 °C, it can be seen that both the ZnO/Fe_2O_3 concentration and the irradiation time significantly influenced the percentage COD removal. The COD removal from the oilfield produce water increases with an increase in the ZnO/Fe_2O_3 concentration (from 1-3 mg/L) and the irradiation time (from 20-180 min). A similar trend is observed when the calcination temperatures were fixed at 500 °C (Figure 7 (a)) and 600 °C (Figure 7(c)). At fixed calcination temperature of 400°C, 500 °C, and 600 °C, the interaction effect of the calcination temperature and the irradiation time resulted in COD removal of 84%, 80%, and 74%, respectively. The ANOVA results summarized in Table 4 shows that the interaction effects of the ZnO/Fe_2O_3 concentration and the irradiation time on the COD removal are statistically significant since the p-value is less than 0.05.

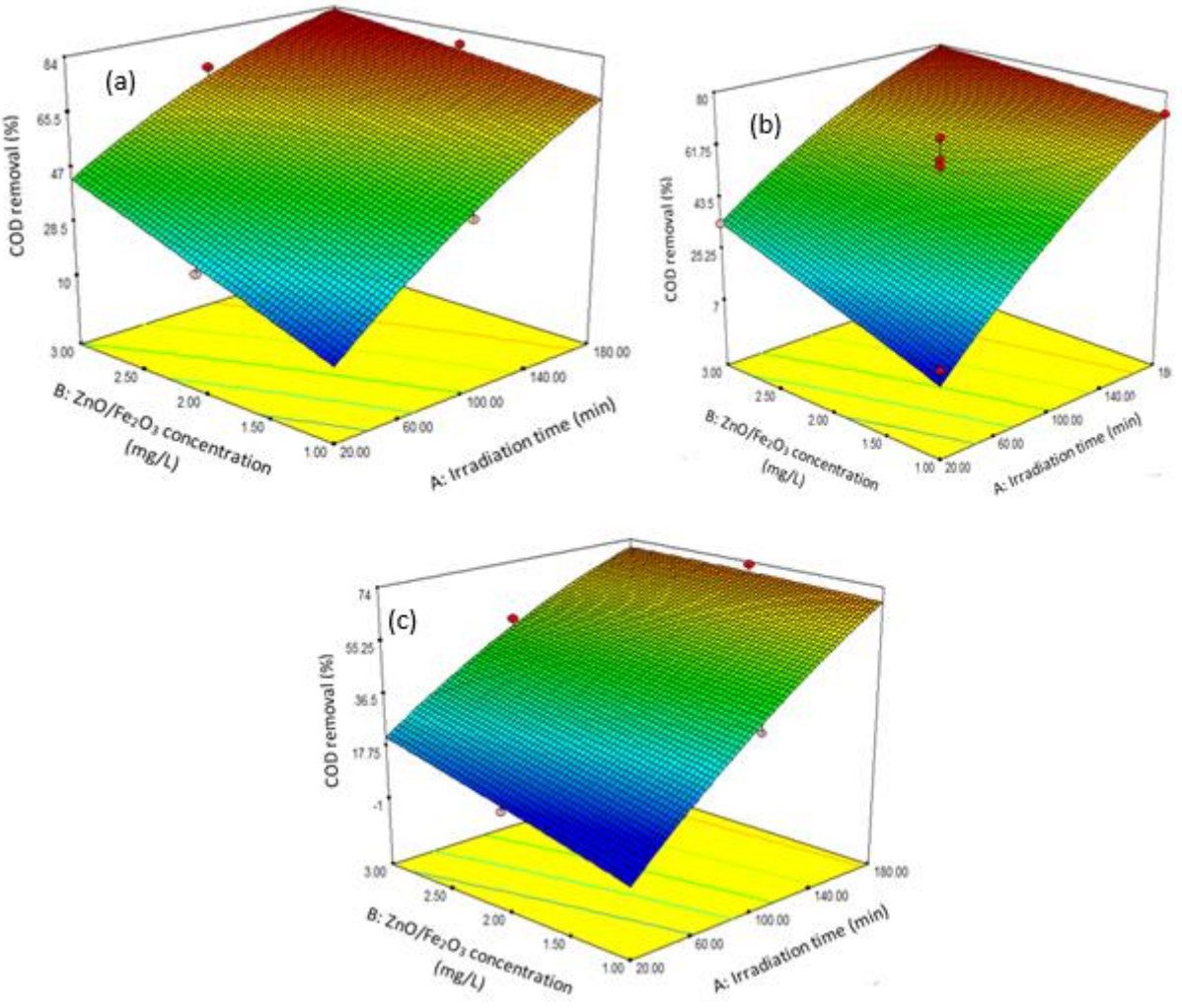

Fig. 7. Interaction effect of ZnO/ Fe_2O_3 concentration and irradiation time on the COD removal fixing the calcination temperature at (a) 400 °C (b) 500 °C (c) 600 °C

Figure 8 show the interaction effects of irradiation time (min) and the calcination temperature of the ZnO/Fe_2O_3 nanocomposite on the percentage COD removal fixing the ZnO/Fe_2O_3 concentration. The 3-D plots show that both the irradiation time and the calcination temperature have significant effects on the COD removal. The increase in both the irradiation time resulted in a corresponding

increase in the COD removal. On the contrary, there was a gradual decrease in the percentage COD removal as the calcination temperature of the ZnO/Fe_2O_3 nanocomposite increases. However, based on visual observation, it is obvious that the irradiation time has a higher significant effect on the COD removal compare to calcination temperature. At fixed ZnO/Fe_2O_3 concentrations of 1 mg/L, 2mg/L and 3 mg/L, a corresponding COD removal of 72%, 80% and 83%, were obtained respectively. The ANOVA results summarized in Table 5 shows that the interaction between irradiation time and the calcination temperature have significant effects on the COD removal as indicated by the p-value which is less than 0.05.

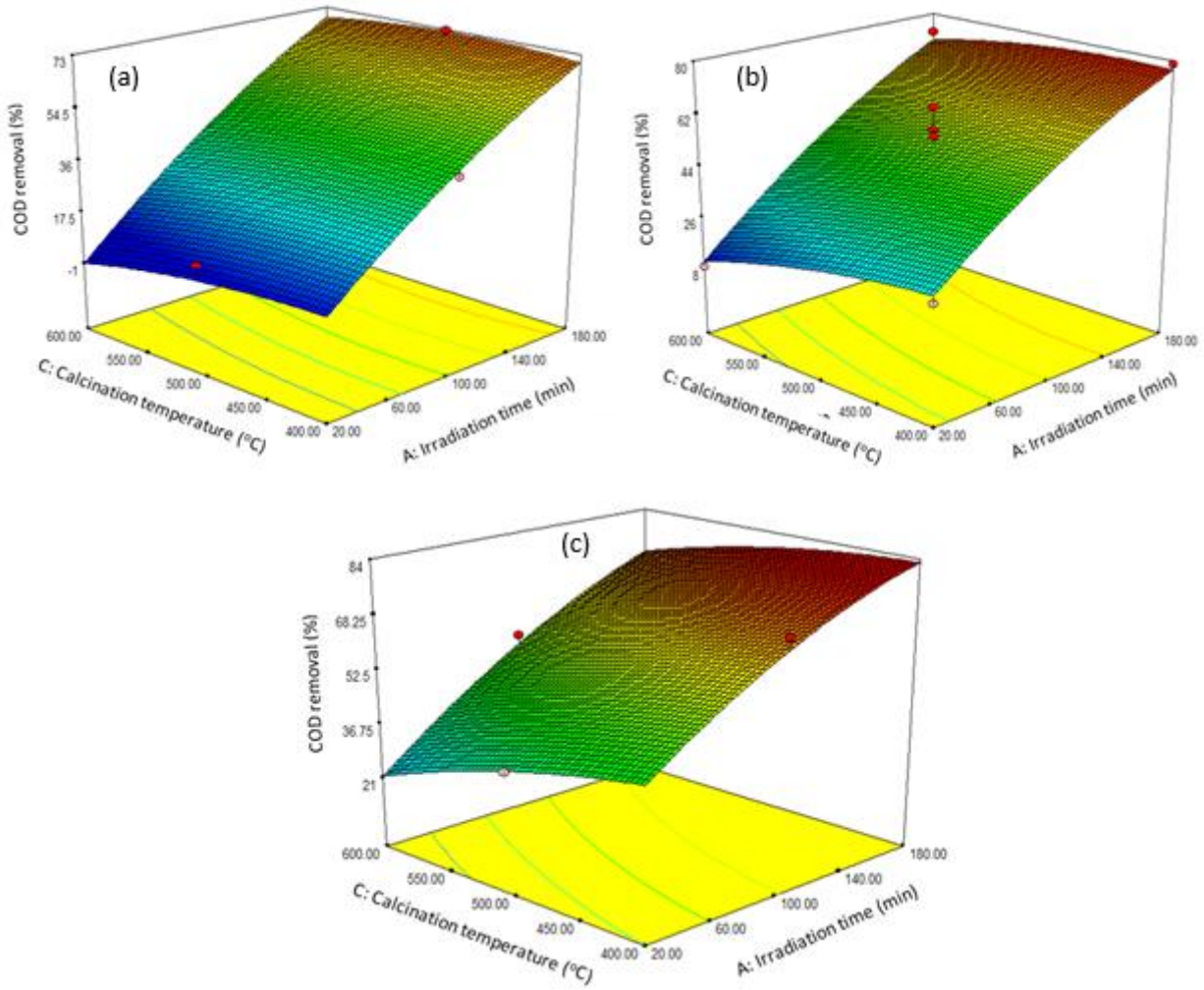

Fig. 8. Interaction effect of calcination temperature and irradiation time on the COD removal fixing the ZnO/ Fe_2O_3 concentration at (a) 1 mg/L (b) 2 mg/L (c) 3 mg/L

The interaction effect of ZnO/Fe_2O_3 concentration and the calcination temperature of the ZnO/Fe_2O_3 nanocomposite on the percentage COD removal fixing the irradiation time is depicted in Figure 9. A significant effect can be observed on the interaction between the ZnO/Fe_2O_3 concentration and the calcination temperature. However, the individual effects show that an increase in the calcination temperature of the ZnO/Fe_2O_3 nanocomposite resulted in a decrease in the percentage COD removal. On the other hand, the increase in the ZnO/Fe_2O_3 concentration resulted in a corresponding increase in the percentage COD removed. Based on the ANOVA analysis (p-value < 0.05), the interaction effect on the ZnO/Fe_2O_3 concentration and the calcination temperature of the ZnO/Fe_2O_3 nanocomposite is statistically significant. At fixed irradiation time of

20 min, 100 min, and 180 min, 44%, 72%, and 82.8% of COD were removed from the oilfield produce water.

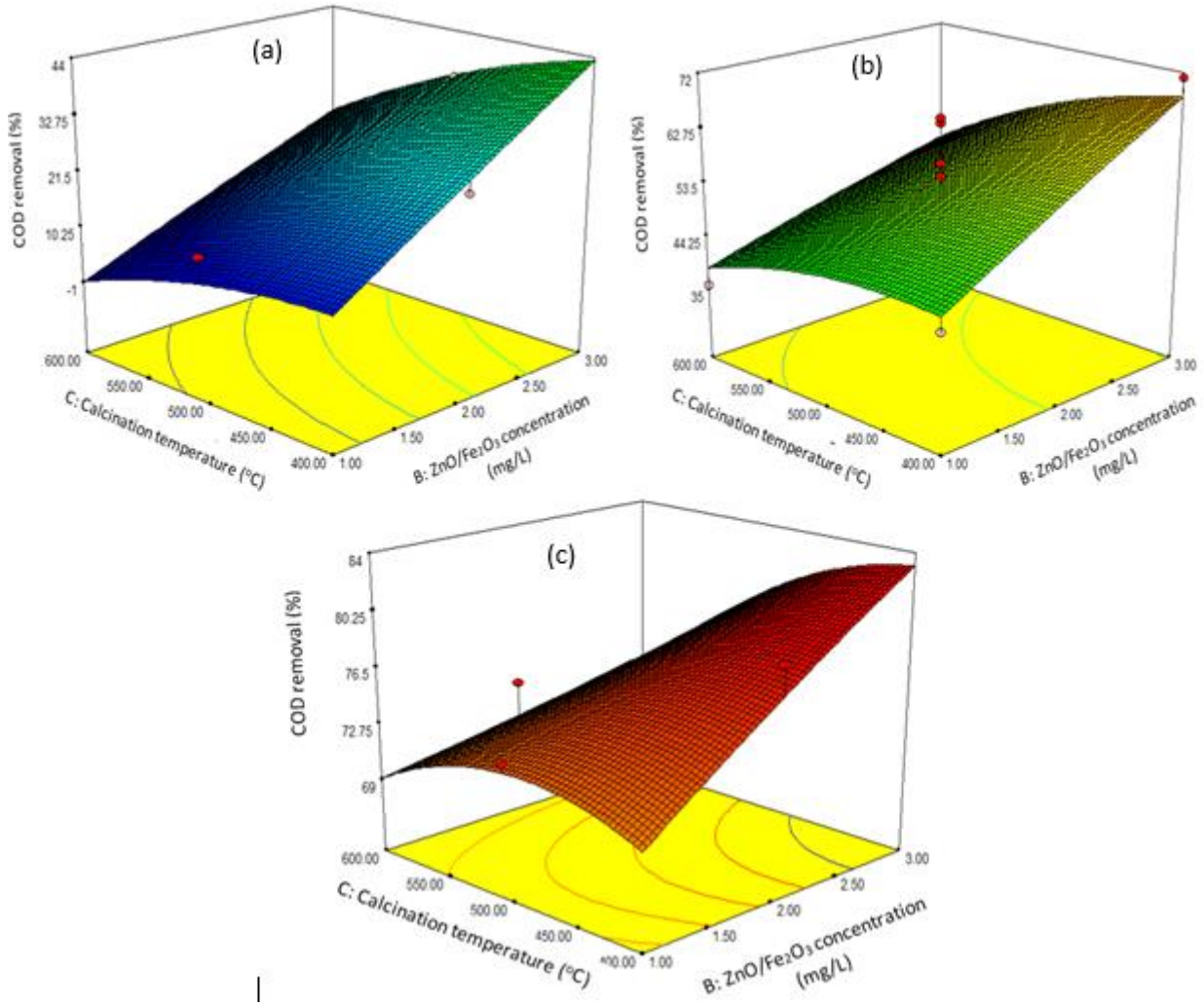

Fig. 9. Interaction effect of calcination temperature and ZnO/ Fe_2O_3 concentration on the COD removal fixing the irradiation time at (a) 20 min (b) 100 min (c) 180 min

Overall, based on the model fitting statistics summarized in Table 4, Model analysis in Table 5, and analysis of variance in Table 6, it can be seen that the 2-factor interaction (2FI) has a very high coefficient of determination (R^2) of 0.959 and adjusted R^2 of 0.935. This is an indication of the strong correlation between each of the parameters as they affect the percentage of COD removal. Although, the statistical analysis also shows that there is a linear-effects on the parameters on the percentage COD removal which is also confirmed from the model analysis with a p-value less than 0.0001.

Table 4
Model Fitting Statistics for the removal of COD from the oil field produced water

Source	Standard deviation	R^2	Adjusted R^2	Predicted R^2	PRESS
Linear	5.270	0.948	0.936	0.901	684.315
2FI	5.313	0.959	0.935	0.833	1153.50
Quadratic	4.279	0.981	0.958	0.712	1986.84
Cubic	1.053	0.999	0.997		+

Table 5
Model analysis

Source	Sum of Squares	degree of freedom	Mean Square	F-Value	p-value, Prob > F
Mean vs Total	41226.68	1	41226.68		
Linear vs Mean	6534.82	3	2178.27	78.44	< 0.0001
2FI vs Linear	78.74	3	26.25	0.93	0.4617
Quadratic vs 2FI	154.09	3	51.36	2.81	0.1179
Cubic vs Quadratic	123.74	3	41.25	37.20	0.0022
Residual	4.44	4	1.11		
Total	48122.52	17	2830.74		

Table 6
Analysis of Variance (ANOVA) for the COD removal from the oilfield produced water

Source Model	Sum of Squares	Degree of freedom	Mean Square	F-Value	p-value, Prob > F	
	6767.66	9	751.96	41.0653	< 0.0001	significant
A-Irradiation Time	5446.55	1	5446.55	297.441	< 0.0001	
B-ZnO/Fe_2O_3 concentration	812.85	1	812.85	44.3905	0.0003	
C-Calcination Temperature	275.42	1	275.42	15.041	0.0061	
AB	24.35	1	24.35	1.33001	0.0287	
AC	24.85	1	24.85	1.35709	0.0282	
BC	29.54	1	29.54	1.61316	0.0245	
A^2	135.57	1	135.57	7.40342	0.0297	
B^2	7.55	1	7.55	0.41242	0.5412	
C^2	3.52	1	3.52	0.1922	0.6743	
Residual	128.18	7	18.31			
Lack of Fit	106.30	3	35.43	0.54387	0.6779	not significant
Pure Error	260.61	4	65.15			
Cor Total	7552.56	16				

3.3 Interaction Effects of The Process Parameters on The Percentage Phenol Removal

The interaction effects of the three process parameters on the percentage of phenol removal were also investigated. Figure 10-12 show 3-D plots of the effect of interaction of these parameters on the percentage phenol removal. In Figure 10, it can be seen that there was a significant effect from the interaction between the irradiation time and the ZnO/Fe_2O_3 concentration at fixed calcination temperature. At fixed calcination temperature of 400 ^oC, 500 ^oC, and 600 ^oC, the interaction effect between the irradiation time and the ZnO/Fe_2O_3 concentration resulted in a corresponding phenol removal of 98.9%, 88.9%, and 69.8%, respectively. There was an increase in the percentage of phenol removed from oilfield produced water as the irradiation time increases. However, a gradual decrease was observed in the percentage of phenol removed from the oilfield produced water as the calcination temperature of the ZnO/Fe_2O_3 nanocomposite increases. The ANOVA results shown in Table 7 revealed that the interaction between the irradiation time and the ZnO/Fe_2O_3 concentration is statistically significant since the p-value is approximately equal to 0.05.

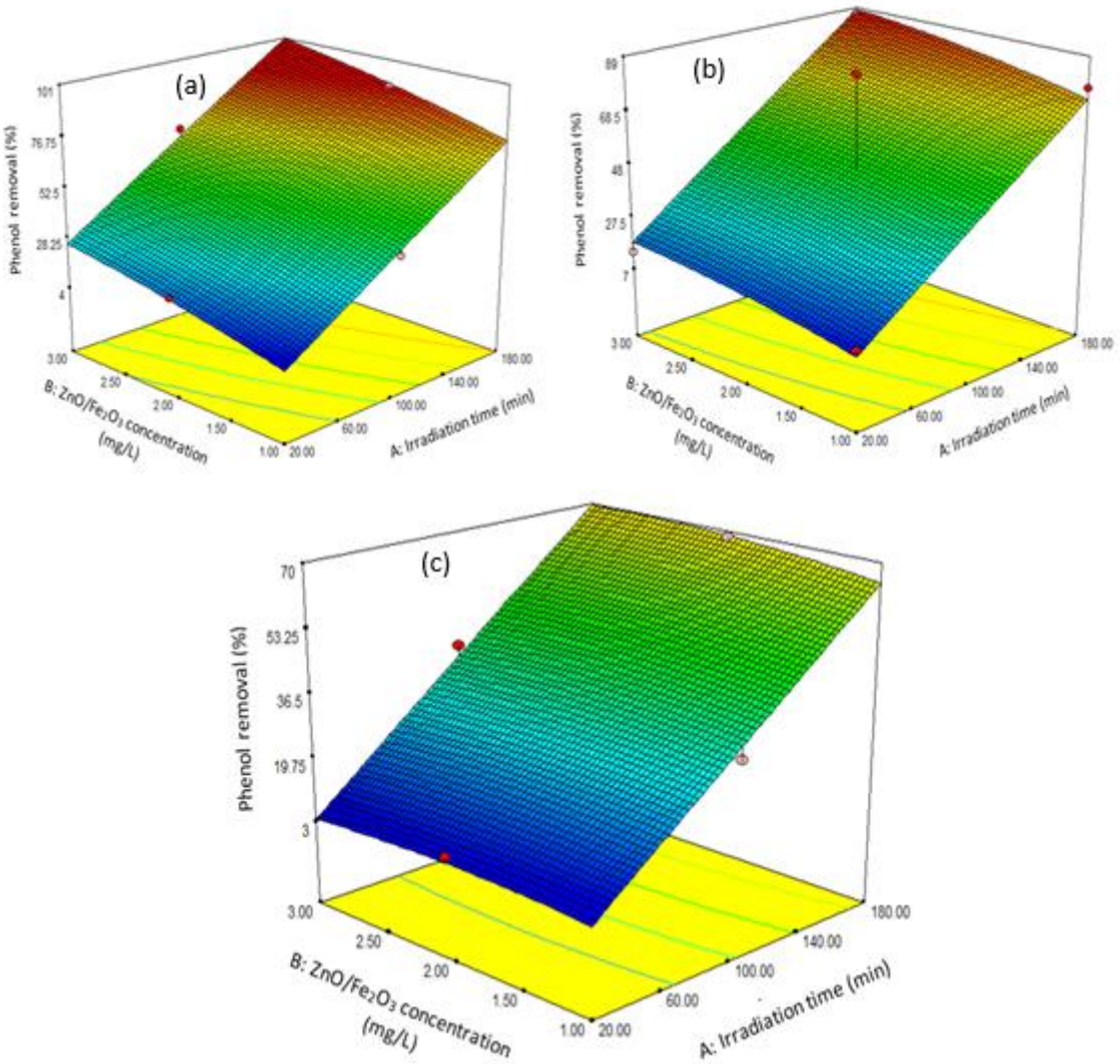

Fig. 10. Interaction effect of irradiation time and ZnO/ Fe_2O_3 concentration on the Phenol removal fixing the calcination temperature at (a) 400 °C(b) 500 °C (c) 600 °C

Figure 11 shows the effects of interaction between irradiation time and calcination temperature of the ZnO/Fe_2O_3 nanocomposite on the percentage removal of phenol from the oilfield produced water at fixed values of ZnO/Fe_2O_3 concentrations. Both the irradiation time and calcination temperature of the ZnO/Fe_2O_3 nanocomposite significantly influence the phenol removal from the oilfield produced water. However, a close look at the individual effect of the parameters revealed that an increase in the irradiation time from 20 to 180 min resulted in a drastic increase in the percentage phenol removal from the oilfield produced water. Conversely, an increase in the calcination temperature of the ZnO/Fe_2O_3 nanocomposite resulted in a decrease in the percentage phenol removal. At fixed ZnO/Fe_2O_3 concentration of 1, 2, and 3mg/L, the highest percentage phenol removal of 76.7%, 88.8%, and 98.7%, respectively were obtained. The ANOVA results show that the interaction between the irradiation time and calcination temperature of the ZnO/Fe_2O_3 nanocomposite is statistically significant since the p-value is less than 0.05. This implies there is over 95 % confidence level on the interaction effects of the two parameters understudied.

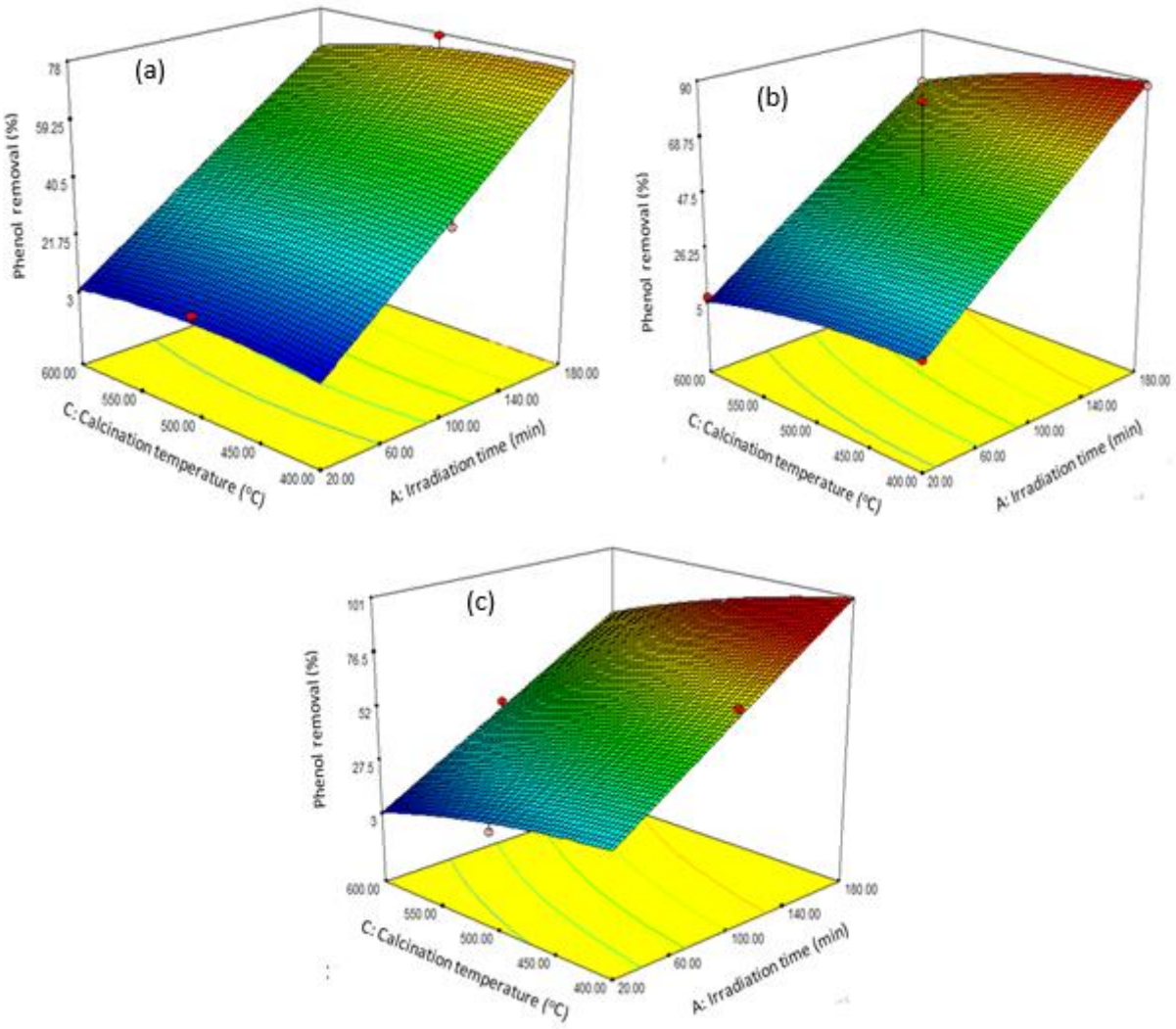

Fig. 11. Interaction effect of calcination temperature and irradiation time on the Phenol removal fixing the ZnO/ Fe_2O_3 concentration at (a) 1 mg/L (b) 2 mg/L (c) 3 mg/L

Figure 12 shows the effect of interaction between ZnO/ Fe_2O_3 concentration and calcination temperature of the nanocomposite. The interaction between the ZnO/ Fe_2O_3 concentration and calcination temperature of the nanocomposite significantly influences the percentage phenol removal as indicated by the p-value of 0.018 obtained from the ANOVA result. Based on the individual effect, there was a sharp increase in the percentage removal of the phenol from the oilfield produced water. At fixed irradiation time of 20 min, 100 min, and 180 min, the highest percentage phenol removal of 25.7%, 63.5%, and 97.8%, respectively were obtained from the 3-D plots. Based on the individual effect, an increase in the calcination temperature of the ZnO/Fe_2O_3 nanocomposite at fixed irradiation time of 20 min resulted in a gradual rise in the percentage phenol removal until it reaches climax and thereafter declined. A similar trend was reported when the temperature was fixed at 100 min and 180 min.

The model summary statistic, the fit summary, and ANOVA in Table 7- 9, respectively, show that the two-factor interaction (2FI) were statistically significant since the p-value is less than 0.05 which is an indication that a high confidence level greater than 95%. Besides, the R^2 values of 0.988 indicate that there is a strong correlation between the parameters. The statistical analysis also indicated that the linear interaction between the different parameters is also statistically significant since the p-value is less than 0.05 which can also the corroborated by the high value of R^2 (0.975).

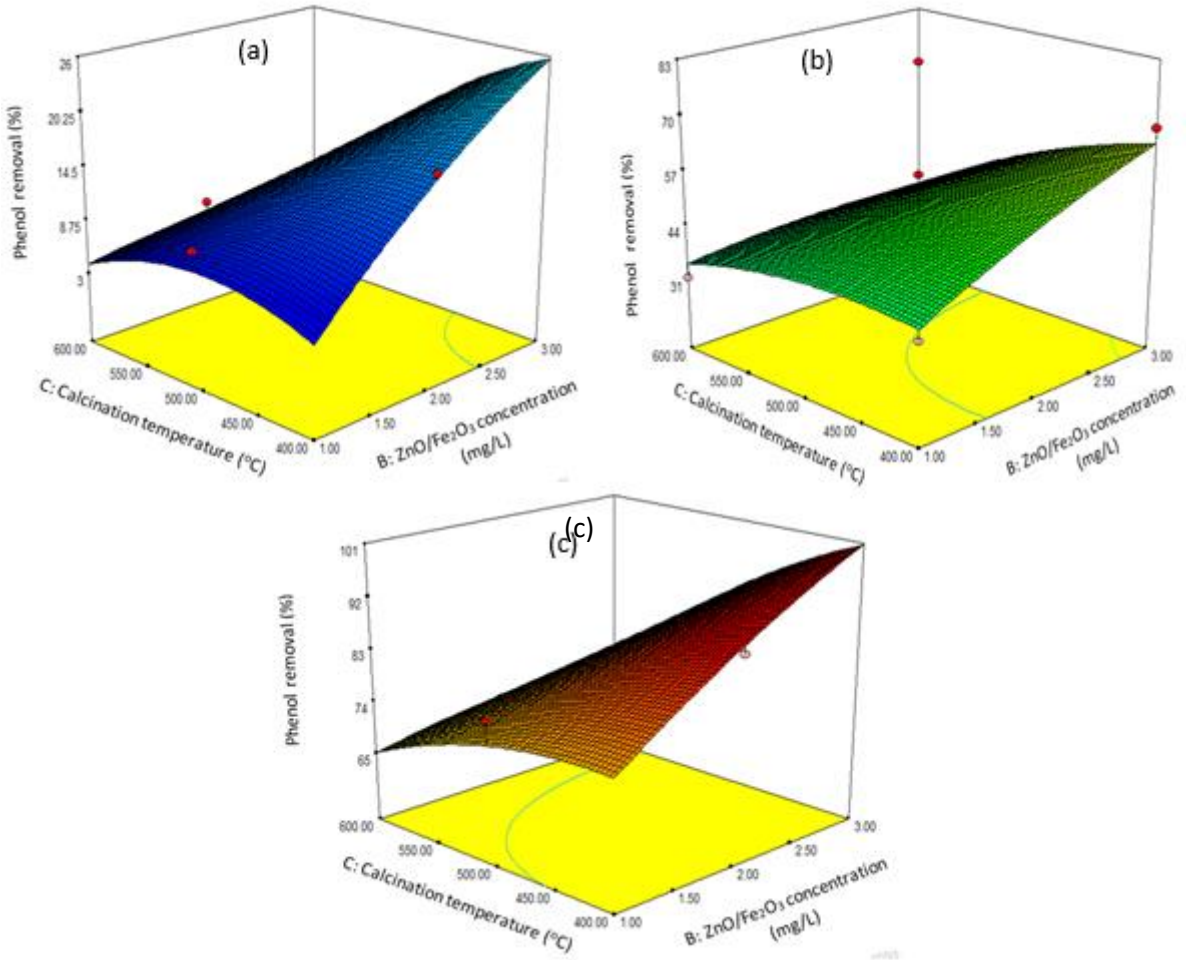

Fig. 12. Interaction effect of calcination temperature and ZnO/ Fe_2O_3 concentration on the Phenol removal fixing the irradiation time at (a) 20 min (b) 100 min (c) 180 min

Table 7
Model summary statistics

Source	Standard Deviation	R^2	Adjusted R^2	Predicted R^2	PRESS
Linear	4.480	0.975	0.969	0.949	530.813
2FI	3.490	0.988	0.981	0.946	562.316
Quadratic	3.480	0.992	0.981	0.871	1342.07
Cubic	0.498	1.000	1.000		+

Table 8
Fit Summary

Source	Sum of Squares	degree of freedom	Mean Square	F-Value	p-value, Prob > F
Mean vs Total	33762.22	1	33762.22		
Linear vs Mean	10102.95	3	3367.65	167.81	< 0.0001
2FI vs Linear	139.07	3	46.36	3.81	0.0469
Quadratic vs 2FI	37.05	3	12.35	1.02	0.4395
Cubic vs Quadratic	83.78	3	27.93	112.61	0.0003
Residual	0.99	4	0.25		
Total	44126.06	17	2595.65		

Table 9
Analysis of Variance (ANOVA) for phenol degradation

	Sum of Squares	degree of freedom	Mean Square	F-Value	p-value, Prob > F	
Source model	10279.06	9	1142.12	94.31	< 0.0001	significant
A-Irradiation Time	9261.61	1	9261.61	764.75	< 0.0001	
B-ZnO/Fe_2O_3 conc	321.31	1	321.31	26.53	0.0013	
C-Calcination Temperature	520.03	1	520.03	42.94	0.0003	
AB	6.00	1	6.00	0.50	0.0504	
AC	20.70	1	20.70	1.71	0.0232	
BC	112.36	1	112.36	9.28	0.0187	
A^2	28.57	1	28.57	2.36	0.1684	
B^2	6.90	1	6.90	0.57	0.4750	
C^2	0.20	1	0.20	0.02	0.9004	
Residual	84.77	7	12.11			
Lack of Fit	83.78	3	27.93	0.08	0.9700	not significant
Pure Error	1480.55	4	370.14			
Cor Total	11861.62	16				

4. Conclusion

The use of ZnO/Fe_2O_3 nanocomposite photocatalyst synthesized by the sol-gel method for the photodegradation of phenol in oilfield produced water has been investigated. The characterization of the ZnO/Fe_2O_3 nanocomposite photocatalyst using different instrument techniques shows that the nanocomposite exhibits appropriate physicochemical and photo-properties suitable for photocatalytic activity. The individual and interaction effect of irradiation time, ZnO/Fe_2O_3 concentration, and calcination temperature of the ZnO/Fe_2O_3 nanocomposite investigated using BBDoE revealed that all the parameters significantly influence the percentage COD removal and phenol degradation. Based on the ANOVA, the irradiation time (p-value < 0.0001) was adjudged to have the most significant effect of the percentage COD removal and phenol degradation compared to calcination temperature of the ZnO/Fe_2O_3 nanocomposite (p-value = 0.0003) and ZnO/Fe_2O_3 concentration (p-value = 0.0013). The interaction between the ZnO/Fe_2O_3 concentration and the calcination temperature of the ZnO/Fe_2O_3 nanocomposite was found to produce the most significant effects on the percentage COD removal and phenol degradation. This study has demonstrated that irradiation time, ZnO/Fe_2O_3 concentration and calcination temperature of the ZnO/Fe_2O_3 nanocomposite are important parameters to be considered in a scale-up scenario of photocatalytic degradation of phenol in oilfield produced water. Hence, the full understanding of the interaction pattern of these process variables will serve as a guide in designing a suitable photo-reactor that could be employed for degrading phenols in oil produce water.

References

[1] Fakhru'l-Razi, Ahmadun, Alireza Pendashteh, Luqman Chuah Abdullah, Dayang Radiah Awang Biak, Sayed Siavash Madaeni, and Zurina Zainal Abidin. "Review of technologies for oil and gas produced water treatment." *Journal of hazardous materials* 170, no. 2-3 (2009): 530-551. https://doi.org/10.1016/j.jhazmat.2009.05.044

[2] Munirasu, Selvaraj, Mohammad Abu Haija, and Fawzi Banat. "Use of membrane technology for oil field and refinery produced water treatment—A review." *Process safety and environmental protection* 100 (2016): 183-202. https://doi.org/10.1016/j.psep.2016.01.010

[3] Zheng, Jisi, Bing Chen, Worakanok Thanyamanta, Kelly Hawboldt, Baiyu Zhang, and Bo Liu. "Offshore produced water management: A review of current practice and challenges in harsh/Arctic environments." *Marine pollution bulletin* 104, no. 1-2 (2016): 7-19. https://doi.org/10.1016/j.marpolbul.2016.01.004

[4] Neff, Jerry M. *Bioaccumulation in marine organisms: effect of contaminants from oil well produced water*. Elsevier, 2002. https://doi.org/10.1016/B978-008043716-3/50002-6

[5] Babich, H., and D. L. Davis. "Phenol: A review of environmental and health risks." *Regulatory Toxicology and Pharmacology* 1, no. 1 (1981): 90-109. https://doi.org/10.1016/0273-2300(81)90071-4

[6] Bruce, Robert M., Joseph Santodonato, and Michael W. Neal. "Summary review of the health effects associated with phenol." *Toxicology and Industrial Health* 3, no. 4 (1987): 535-568. https://doi.org/10.1177/074823378700300407

[7] World Health Organization. "Phenol Health and safety Guide No. 88." (1994).

[8] Xu, Pei, Jörg E. Drewes, Dean Heil, and Gary Wang. "Treatment of brackish produced water using carbon aerogel-based capacitive deionization technology." *Water research* 42, no. 10-11 (2008): 2605-2617. https://doi.org/10.1016/j.watres.2008.01.011

[9] Beall, Gary W. "The use of organo-clays in water treatment." *Applied Clay Science* 24, no. 1-2 (2003): 11-20. https://doi.org/10.1016/j.clay.2003.07.006

[10] Wang, Shaobin, and Yuelian Peng. "Natural zeolites as effective adsorbents in water and wastewater treatment." *Chemical engineering journal* 156, no. 1 (2010): 11-24. https://doi.org/10.1016/j.cej.2009.10.029

[11] Wandera, Daniel, Heath H. Himstedt, Milagro Marroquin, S. Ranil Wickramasinghe, and Scott M. Husson. "Modification of ultrafiltration membranes with block copolymer nanolayers for produced water treatment: The roles of polymer chain density and polymerization time on performance." *Journal of membrane Science* 403 (2012): 250-260. https://doi.org/10.1016/j.memsci.2012.02.061

[12] Bayati, Fatemeh, Jalal Shayegan, and Abolfazl Noorjahan. "Treatment of oilfield produced water by dissolved air precipitation/solvent sublation." *Journal of Petroleum Science and Engineering* 80, no. 1 (2011): 26-31. https://doi.org/10.1016/j.petrol.2011.10.001

[13] Lu, Mang, Zhongzhi Zhang, Weiyu Yu, and Wei Zhu. "Biological treatment of oilfield-produced water: A field pilot study." *International Biodeterioration & Biodegradation* 63, no. 3 (2009): 316-321. https://doi.org/10.1016/j.ibiod.2008.09.009

[14] Guo, Chunmei, Yi Chen, Jinfu Chen, Xiaojun Wang, Guangqing Zhang, Jingxiu Wang, Wenfeng Cui, and Zhongzhi Zhang. "Combined hydrolysis acidification and bio-contact oxidation system with air-lift tubes and activated carbon bioreactor for oilfield wastewater treatment." *Bioresource technology* 169 (2014): 630-636. https://doi.org/10.1016/j.biortech.2014.07.018

[15] Cakir, F. Y., and M. K. Stenstrom. "Greenhouse gas production: a comparison between aerobic and anaerobic wastewater treatment technology." *Water research* 39, no. 17 (2005): 4197-4203. https://doi.org/10.1016/j.watres.2005.07.042

[16] Gupta, V. K., R. Jain, T. Saleh, A. Nayak, and S. Malathi. "Agarwal." *Equilibrium and Thermodynamic studies on the removal and recovery of Sfranine-T dye from industrial effluent separation Scince and technology* 46, no. 5 (2011): 839-846. https://doi.org/10.1039/c2ra20340e

[17] Zhang, Yongqiang, Baoyu Gao, Lei Lu, Qinyan Yue, Qian Wang, and Yuyan Jia. "Treatment of produced water from polymer flooding in oil production by the combined method of hydrolysis acidification-dynamic membrane bioreactor–coagulation process." *Journal of Petroleum Science and Engineering* 74, no. 1-2 (2010): 14-19. https://doi.org/10.1016/j.petrol.2010.08.001

[18] Comninellis, Christos, Agnieszka Kapalka, Sixto Malato, Simon A. Parsons, Ioannis Poulios, and Dionissios Mantzavinos. "Advanced oxidation processes for water treatment: advances and trends for R&D." *Journal of Chemical Technology & Biotechnology: International Research in Process, Environmental & Clean Technology* 83, no. 6 (2008): 769-776. https://doi.org/10.1002/jctb.1873

[19] Martinez-Huitle, Carlos A., and Sergio Ferro. "Electrochemical oxidation of organic pollutants for the wastewater treatment: direct and indirect processes." *Chemical Society Reviews* 35, no. 12 (2006): 1324-1340. https://doi.org/10.1039/B517632H

[20] McFarlane, J., W. B. Ridenour, H. Luo, R. D. Hunt, D. W. DePaoli, and R. X. Ren. "Room temperature ionic liquids for separating organics from produced water." *Separation science and technology* 40, no. 6 (2005): 1245-1265. https://doi.org/10.1081/SS-200052807

[21] Lv, Peng, Xiuping Wang, Yuanbo Chen, Xiaoxuan Guo, Anguo Xu, and Zhiqiang Zhao. "Optimization of chemical agents for removing dispersed oil from produced water in Z oilfield." *Petroleum Science and Technology* 35, no. 12 (2017): 1285-1289. https://doi.org/10.1080/10916466.2017.1324486

[22] Abdullah, Norashima, Bamidele Victor Ayodele, Wan Nurdiyana Wan Mansor, and Sureena Abdullah. "Effect of Incorporating TiO2 Photocatalyst in PVDF Hollow Fibre Membrane for Photo-Assisted Degradation of Methylene Blue." *Bulletin of Chemical Reaction Engineering & Catalysis* 13, no. 3 (2018): 588-591. https://doi.org/10.9767/bcrec.13.3.2909.588-591

[23] Mehrjouei, Mohammad, Siegfried Müller, and Detlev Möller. "A review on photocatalytic ozonation used for the treatment of water and wastewater." *Chemical Engineering Journal* 263 (2015): 209-219. https://doi.org/10.1016/j.cej.2014.10.112

[24] Dong, S. Y. "» Feng JL» Fan MH» et al." *Recent developments in heterogeneous photocatalytic water treatment using visible light-responsive photocatalysts: a review* 5 (2015): 14610-14630. https://doi.org/10.1039/C4RA13734E

[25] Ani, I. J., U. G. Akpan, M. A. Olutoye, and B. H. Hameed. "Photocatalytic degradation of pollutants in petroleum refinery wastewater by TiO2-and ZnO-based photocatalysts: recent development." *Journal of Cleaner Production* 205 (2018): 930-954. https://doi.org/10.1016/j.jclepro.2018.08.189

[26] Iqbal, Jibran, Noor S. Shah, Murtaza Sayed, Nawshad Muhammad, Javed Ali Khan, Zia Ul Haq Khan, Fares M. Howari et al. "Deep eutectic solvent-mediated synthesis of ceria nanoparticles with the enhanced yield for photocatalytic degradation of flumequine under UV-C." *Journal of Water Process Engineering* 33 (2020): 101012. https://doi.org/10.1016/j.jwpe.2019.101012

[27] Ahmad, Tausif, Mohamad Azmi Bustam, Muhammad Zulfiqar, Muhammad Moniruzzaman, Alamin Idris, Jibran Iqbal, Hafiz Muhammad Anwaar Asghar, and Sami Ullah. "Controllable phytosynthesis of gold nanoparticles and investigation of their size and morphology-dependent photocatalytic activity under visible light." *Journal of Photochemistry and Photobiology A: Chemistry* 392 (2020): 112429. https://doi.org/10.1016/j.jphotochem.2020.112429

[28] Ahmad, Tausif, Jibran Iqbal, Mohamad Azmi Bustam, Muhammad Zulfiqar, Nawshad Muhammad, Buthaina Mohamed Al Hajeri, Muhammad Irfan, Hafiz Muhammad Anwaar Asghar, and Sami Ullah. "Phytosynthesis of cerium oxide nanoparticles and investigation of their photocatalytic potential for degradation of phenol under visible light." *Journal of Molecular Structure* (2020): 128292. https://doi.org/10.1016/j.molstruc.2020.128292

[29] Vaiano, V., M. Matarangolo, J. J. Murcia, H. Rojas, José Antonio Navío, and M. C. Hidalgo. "Enhanced photocatalytic removal of phenol from aqueous solutions using ZnO modified with Ag." *Applied Catalysis B: Environmental* 225 (2018): 197-206. https://doi.org/10.1016/j.apcatb.2017.11.075

[30] Xie, Juan, Zhao Zhou, Yiwei Lian, Yongjing Hao, Pan Li, and Yu Wei. "Synthesis of α-Fe2O3/ZnO composites for photocatalytic degradation of pentachlorophenol under UV–vis light irradiation." *Ceramics International* 41, no. 2 (2015): 2622-2625. https://doi.org/10.1016/j.ceramint.2014.10.043

[31] Li, Ching-Feng, Chia-Yen Hsu, and Yuan-Yao Li. "NH3 sensing properties of ZnO thin films prepared via sol–gel method." *Journal of Alloys and Compounds* 606 (2014): 27-31. https://doi.org/10.1016/j.jallcom.2014.03.120

[32] Xu, Jing, Haibin Yang, Wuyou Fu, Kai Du, Yongming Sui, Jiuju Chen, Yi Zeng, Minghui Li, and Guangtian Zou. "Preparation and magnetic properties of magnetite nanoparticles by sol–gel method." *Journal of Magnetism and magnetic Materials* 309, no. 2 (2007): 307-311. https://doi.org/10.1016/j.jmmm.2006.07.037

[33] Sing, Kenneth SW, and Ruth T. Williams. "Physisorption hysteresis loops and the characterization of nanoporous materials." *Adsorption Science & Technology* 22, no. 10 (2004): 773-782. https://doi.org/10.1260/0263617053499032

[34] Donohue, M. D., and G. L. Aranovich. "Classification of Gibbs adsorption isotherms." *Advances in colloid and interface science* 76 (1998): 137-152. https://doi.org/10.1016/S0001-8686(98)00044-X

[35] Groen, J. C., L. A. A. Peffer, and J. Pérez-Ramírez. "Microporous mesoporous Mater pore size determination in modified micro-and mesoporous materials." *Pitfalls and limitations in gas adsorption data analysis* 60 (2003): 1-17.
https://doi.org/10.1016/S1387-1811(03)00339-1

[36] Yang, Huaming, Ke Zhang, Rongrong Shi, and Aidong Tang. "Sol–gel synthesis and photocatalytic activity of CeO2/TiO2 nanocomposites." *Journal of the American Ceramic Society* 90, no. 5 (2007): 1370-1374.
https://doi.org/10.1111/j.1551-2916.2007.01540.x

[37] Benrabaa, Rafik, Axel Löfberg, Jesús Guerrero Caballero, Elisabeth Bordes-Richard, Annick Rubbens, Rose-Noelle Vannier, Hamza Boukhlouf, and Akila Barama. "Sol–gel synthesis and characterization of silica supported nickel ferrite catalysts for dry reforming of methane." *Catalysis Communications* 58 (2015): 127-131.
https://doi.org/10.1016/j.catcom.2014.09.019

[38] Ayodele, Bamidele V., and Chin Kui Cheng. "Modelling and optimization of syngas production from methane dry reforming over ceria-supported cobalt catalyst using artificial neural networks and Box–Behnken design." *Journal of Industrial and Engineering Chemistry* 32 (2015): 246-258.
https://doi.org/10.1016/j.jiec.2015.08.021